

O. SCHMIDT<sup>1</sup>  
M. BAUER<sup>2</sup>,  
C. WIEMANN<sup>2</sup>  
R. PORATH<sup>2</sup>  
M. SCHARTE<sup>2</sup>  
O. ANDREYEV<sup>1</sup>  
G. SCHÖNHENSE<sup>1</sup>  
M. AESCHLIMANN<sup>2</sup>

# Time-resolved two photon photoemission electron microscopy

<sup>1</sup> Institut für Physik, Johannes Gutenberg-Universität, 55099 Mainz, Germany

<sup>2</sup> Fachbereich Physik, Universität Kaiserslautern, 67663 Kaiserslautern, Germany

Received: 22 October 2001/Revised version: 10 January 2002

Published online: 7 February 2002 • © Springer-Verlag 2002

**ABSTRACT** Femtosecond, time-resolved two photon photoemission has been used to map the dynamics of photo-excited electrons at a structured metal/semiconductor surface. A photoemission microscope was employed as a spatially resolving electron detector. This novel setup has the potential to visualize variations of hot electron lifetimes in the femtosecond regime on heterogeneous sample surfaces and nanostructures.

**PACS** 78.47.+p; 79.60.-i; 42.65.Re

## 1 Introduction

Since the first experiments nearly two decades ago [1, 2], time-resolved two photon photoemission (TR-2PPE) has been extensively used to study electron dynamics at metal and semiconductor surfaces [3–10]. However, as this technique is a spatially integrating method, it was not possible to systematically investigate, for example, local variations of the electron dynamics or the effect of surface inhomogeneities on the 2PPE process so far. A striking example is the nonlinear enhancement of the integral photoemission yield due to so-called hot spots at surfaces. This effect is the result of the interaction between the exciting intense laser field and surface defects [11]. In addition, there is increasing interest in the specific hot-electron dynamics of spatially heterogeneous systems. TR-2PPE enables meaningful investigation of such systems only under very restricted conditions [12]. The approach we present in this paper to overcome this drawback is the combination of TR-2PPE and photoemission electron microscopy (PEEM), an experimental technique capable of high spatial resolution in the 20-nm regime.

In a TR-2PPE process, a first (pump) pulse populates an intermediate state located between the Fermi edge and the vacuum level, a second (probe) pulse photo-emits these electrons into the vacuum. A defined control of the temporal delay between pump and probe pulses enables information about the decay dynamics of the photo-excited electrons to be captured. As the 2PPE process is a nonlinear photoemission process, the overall photoelectron count rate in the case of

temporal overlap between pump and probe pulses is increased compared to the case in which both pulses are well separated. For identical collinear pulses and optimum spatial overlap, this enhancement results in a peak-to-background ratio of 8 : 1 for interferometric temporal resolution and 3 : 1 for phase-averaging resolution, respectively (see Fig. 1a). A broadening of the autocorrelation trace reflects the finite lifetime of the electron population in the intermediate state.

To obtain information on the energy dependence of lifetimes of excited electrons, TR-2PPE measurements are generally energy-resolved by having an electron-energy analyzer as the detector. For most of the metals and semiconductors investigated so far, the lifetime of excited electrons increases with decreasing excitation energy. Ideally, the lifetime of hot electrons in a free-electron gas is proportional to  $(E - E_F)^{-2}$ , as follows from Fermi-liquid theory [13–17]. For metals, relaxation times down to the low fs regime have been observed. On the other hand, semiconductors (e.g. GaAs) show significantly longer lifetimes due to the restricted phase space for inelastic decay [18].

PEEM as employed here has no significant energy resolution. Therefore, the brightness of a PEEM image is proportional to the total electron yield or the photocurrent. Nevertheless, PEEM is still capable of directly visualizing material-dependent variations in hot-electron lifetimes on heterogeneous sample surfaces, even in this energy-integrating mode. Moreover, a microscopic imaging method reveals inhomogeneities in the lateral distribution of two-photon photoemission, e.g. the presence of “hot-spots” on the sample surface [11, 19].

The purpose of this paper is to present the realization of a new technique (TR-PEEM) that has the potential to allow femtosecond electron dynamics in a nanoscale dimension to be studied.

## 2 Experiment

A schematic of the experimental setup is shown in Fig. 2. The PEEM instrument used for our experiments (FOCUS GmbH, Germany) has an ultimate resolution of about 20 nm and is described in detail in [20]. In brief, the electron-optical column is an electrostatic three-lens system with a contrast aperture and an octopole stigmator. It allows a zoom range from an under 10  $\mu\text{m}$  field-of-view to one of

 Fax: +49-631/205-3903, E-mail: mkbauer@physik.uni-kl.de

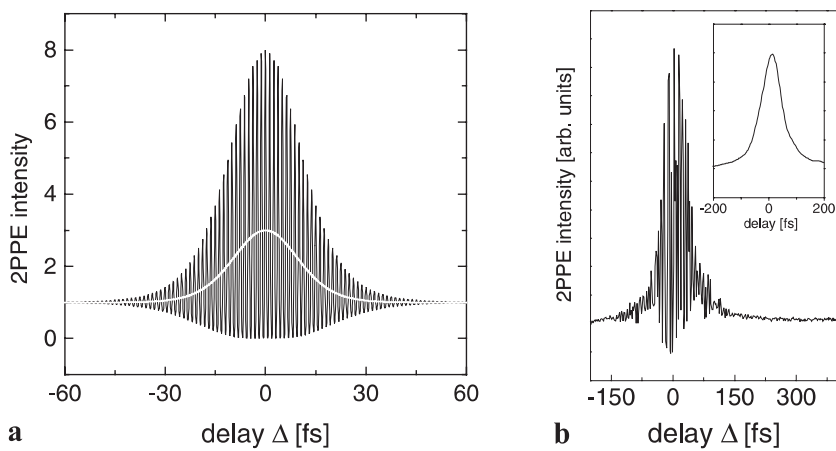


**FIGURE 1** **a** Simulation of a second-order (2PPE) autocorrelation trace; in the case of perfect spatial overlap, interferometric measurements result in a peak-to-background ratio of 8 : 1 (*black line*) and phase-averaged measurements in a ratio of 3 : 1 (*white line*). **b** 2PPE autocorrelation trace from a silver-covered area as obtained with the TR-PEEM apparatus. *Inset*: corresponding phase-averaged correlation trace extracted

about 500  $\mu\text{m}$ . The sample stage is piezomotor driven and integrated into the microscope column. The image is intensified by a multichannel-plate/YAG-screen arrangement. Images are acquired by a slow-scan CCD camera behind the YAG-screen with  $256 \times 256$  pixels. Hence, it employs parallel image acquisition, similar to an optical microscope. It is, therefore, ideally suited for a real-time observation of the spatial electron-yield distribution. Typical exposure times used in this work are in the range of 300 ms to several seconds per image.

Besides a conventional mercury vapor UV source ( $h\nu = 4.9$  eV) a 82-MHz pulsed Ti:sapphire laser, tunable from 750 to 830 nm, was used for photoelectron excitation via two- and multiphoton excitation. The system delivers pulses of up to 9 nJ/pulse with a duration of 40 fs. The linearly polarized output can be frequency-doubled in a 0.2-mm-thick beta barium borate (BBO) crystal to produce pulses at  $h\nu = 3\text{--}3.4$  eV. Both the IR and blue pulses can be focused under  $65^\circ$  incidence to the normal of the sample surface.

For time-resolved measurements the blue pulses were split to equal intensity pump and probe pulses and later combined collinearly by a second beam-splitter. The probe pulse can be delayed with respect to the pump pulse by a computer-

controlled delay stage. In this mode a series of images is taken at varying temporal delays between the two beams.

Samples for lifetime contrast measurements were prepared by evaporation of an overlayer material onto a substrate. The substrates were masked by a fine mesh during the evaporation in order to obtain a structured film. Prior to evaporation, the substrates were prepared by etching to remove oxide layers. After transfer to the vacuum chamber, they were cleaned by annealing to  $480^\circ\text{C}$ . Our investigation focused on patterned silver films on the semiconductor substrates silicon and gallium arsenide. We expected that the significant difference in the carrier dynamics between semiconductors and metals would result in a visible lifetime contrast between these materials, even for energy-integrating measurements.

We used two different approaches to data analysis. In the decay mode, we used images taken at different temporal overlaps of the pump and probe pulses (e.g. 0-fs and 60-fs delay) and calculated the ratio

$$I(\text{lifetime}) \propto \frac{I(60 \text{ fs}) - I(\infty)}{I(0 \text{ fs}) - I(\infty)} \quad (1)$$

for every image pixel.  $I(0 \text{ fs})$ ,  $I(60 \text{ fs})$ , and  $I(\infty)$  denote the brightness values of the corresponding pixels of images taken at zero delay, at 60 fs, and at a large (infinite) delay, respectively. Note that it is important to subtract a background image taken at infinite delay from the other images prior to forming their ratio. Otherwise the background contribution from photoemission by the single pulses results in additional contrast not reflecting the actual difference in the excited electrons' lifetimes.

In the FWHM mode the photoemission intensity from each pixel of the image is plotted as a function of delay between the pump and probe pulses. A resulting autocorrelation trace is shown in Fig. 1b. The high-frequency components of the trace can be filtered numerically, resulting in the phase-averaged autocorrelation trace (see inset). The FWHM extracted from these autocorrelation traces reflect the lateral distribution of differences in the relaxation dynamics and can be displayed in terms of an FWHM map. For sufficiently small scan steps (160 as) a stable fringe pattern with a periodicity of 1.3 fs corresponding to the frequency of the exciting 400-nm light was observed. This indicates that the setup is, in principle, capable of performing interferometric, spatio-temporal, high-resolution measurements.

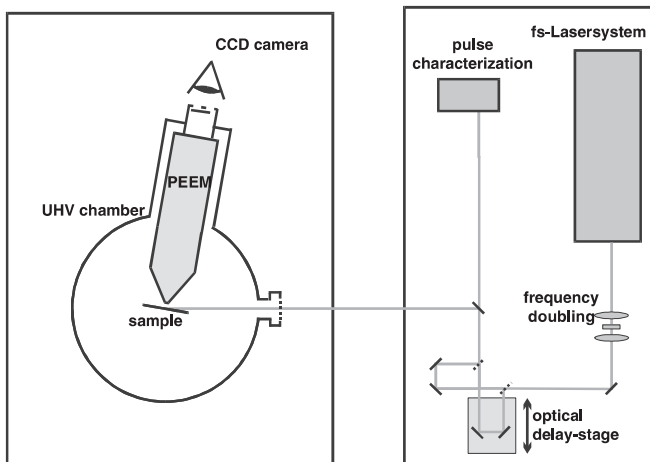


**FIGURE 2** Schematic of the experimental setup used for the TR-PEEM experiment

### 3 Results

#### 3.1 Nonlinear PEEM

An important issue in the interpretation of TR-2PPE data is the question regarding from which area of the sample electrons are actually photo-emitted. This local information can be related to the measured electron dynamics in spatially integrating experiments. In contrast to 1PPE this is a critical parameter due to the nonlinearity of a 2PPE process. Field enhancement at steps, edges or tips can very efficiently increase the photoemission signal from a sample and might finally dominate the overall electron yield, even if the effective area of these structures is small. While for a well-prepared single-crystal surface a rather homogeneous photoemission signal can be assumed, it becomes definitely a problem as soon as one deals with heterogeneous (e.g. nanostructured) samples. For example, it is expected that by a defined manipulation of the sample structure on a nanoscale, the electron dynamics can be tuned in a specific way. It is obvious that knowledge of the source region of the electrons is essential for a reliable interpretation of experimental data.

How inhomogeneities at a surface can result in dramatic space selectivity in nonlinear photoemission becomes obvious from Fig. 3: It shows images of a patterned silver film on silicon ([100] orientation). The field of view is about  $40\ \mu\text{m}$  in diameter. Figure 3a was taken in conventional PEEM mode using a mercury-vapor UV source. It shows the lateral distribution of one-photon photoemission near the photo-threshold. Figure 3b and c were taken with the fs-pulsed laser beam using the second harmonic and the fundamental wavelength of the laser, respectively. They display the lateral distributions of two-photon and three-photon photoemission. Note that the field-of-view displayed in Fig. 3a is different from that in Fig. 3b and c, which is due to a slight sample movement between the acquisition of the images. The faint dark lines result from defects in the multichannel plate.

It is noticeable that the lateral distribution of the photoemission intensity strongly depends on the number of photons absorbed in the elementary photoemission process. Except for a few bright spots, the silver patches appear uniformly bright in Fig. 3a, taken with the UV lamp ( $h\nu = 4.9\ \text{eV}$ , one-photon photoemission). In Fig. 3b, taken with the second harmonic of the laser (400-nm wavelength,  $h\nu = 3.1\ \text{eV}$ ; two-photon photoemission), the topography of the island-like silver film becomes visible. The image brightness is less uniform and exhibits many bright spots in the Ag pattern. Finally, in the image taken with the fundamental wavelength of the laser (800 nm,  $h\nu = 1.55\ \text{eV}$ ), the photoemission intensity is concentrated in only a few very bright spots. The background homogenous gray level has practically disappeared. In addition, the material contrast between Ag and Si is completely absent in Fig. 3c. This phenomenon can be attributed to local field enhancement at roughness features and is responsible for other effects such as surface-enhanced Raman scattering or enhanced second-harmonic generation from rough silver films [11, 21–26]. In the PEEM image, these bright spots exhibit a characteristic dependence on the laser polarization [19].

#### 3.2 Time-resolved PEEM

Figure 4 summarizes results from a TR-PEEM scan. The sample chosen here is silver evaporated onto a masked gallium-arsenide substrate, (100) surface, in the same manner as the silver/silicon sample. A single pixel in these images corresponds to an area of about  $0.09\ \mu\text{m}^2$ . Figure 4a is a 2PPE image and shows the patterned silver film (hexagonal patches), having the same geometry as the one shown in Fig. 3. Note that the brightness values of the different areas are approximately equal. Figure 4c, left, shows a “decay image” obtained from an image-processing procedure (as described above) calculated for 60-fs delay. Corresponding to (1), the darker appearance of the hexagons reflects

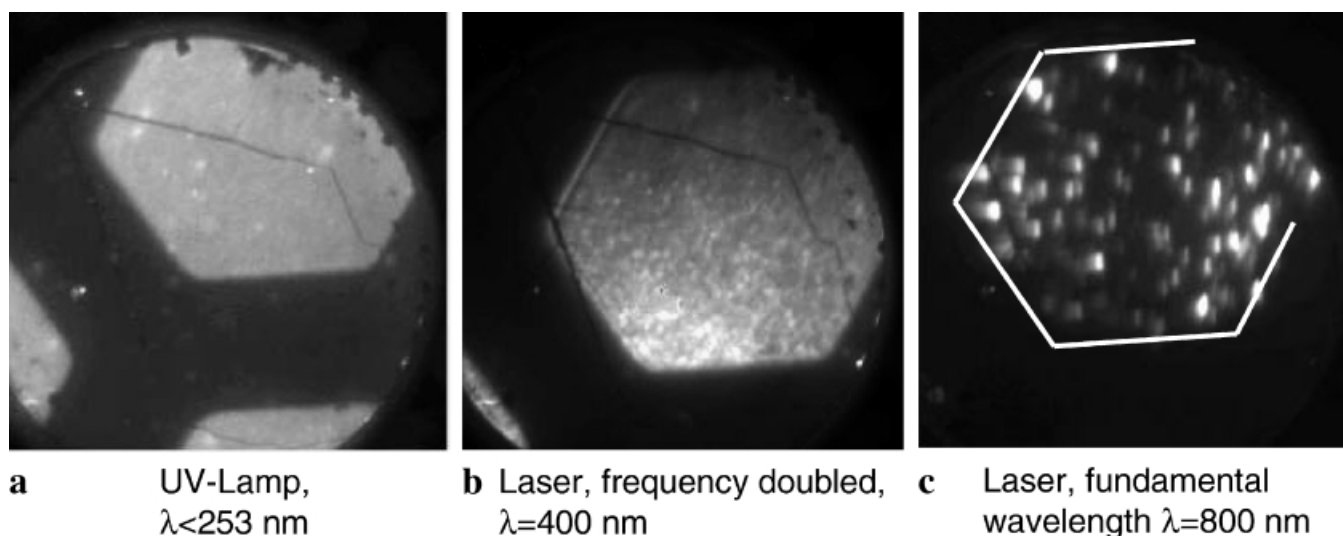


**FIGURE 3** PEEM images of a patterned silver film (*hexagon-shaped patches*) on silicon taken with different excitation sources (field-of-view:  $60\ \mu\text{m}$ ). **a** PEEM image taken with a UV lamp; spatial distribution of one-photon photoemission. **b** PEEM image taken with a frequency-doubled Ti:sapphire laser,  $\lambda = 400\ \text{nm}$ ; spatial distribution of two-photon photoemission. **c** PEEM image taken with the fundamental wavelength of the Ti:sapphire laser,  $\lambda = 800\ \text{nm}$ ; spatial distribution of three-photon photoemission; the *white lines* indicate the position of the silver hexagon

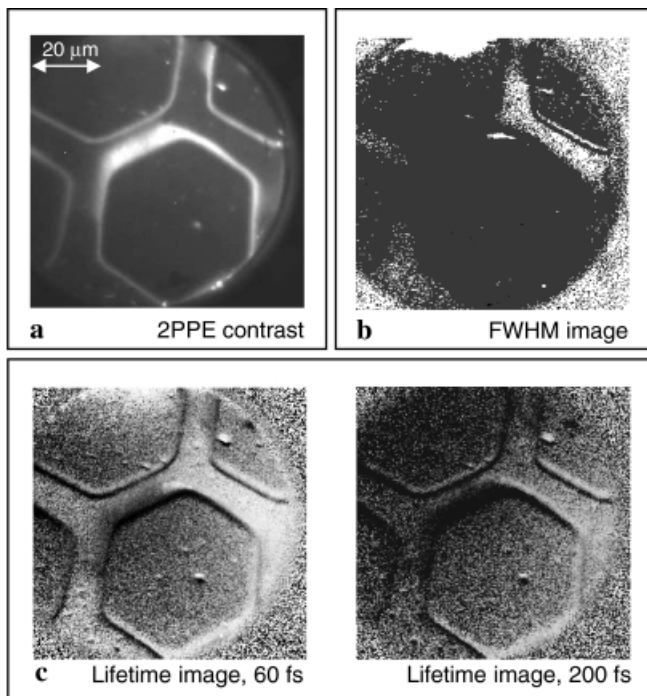


**FIGURE 4** TR-2PPE microscopy of silver on gallium arsenide. **a** PEEM image of the microstructured Ag layer (partly visible hexagonal patches) taken with 400-nm laser radiation. **b** FWHM image extracted from a pump-probe PEEM scan of the same area. The brightness value of each pixel corresponds to the FWHM of the respective autocorrelation trace. **c** *Left*: Processed image by means of (1) exhibiting differences in the lifetime (decay image) calculated for 60-fs delay (areas having shorter hot-electron lifetimes appear darker in the image); *right*: decay image for 200-fs delay

a shorter hot-electron lifetime of silver in comparison to the GaAs interstitial parts. Additional relief-like contrast visible at the edges of the silver patches arises from sample movement during measurement, which causes the images used for extraction of the lifetime map to show slightly different areas. For comparison Fig. 4c, right, shows a “decay image” corresponding to a delay of 200 fs. It is obvious that at this large delay, where most of the excited population has decayed in both materials, the lifetime contrast is significantly weakened. The observed contrast between silver and GaAs is also reproduced in the FWHM image shown in Fig. 4b. Again, the silver hexagons appear dimmer in comparison to the GaAs areas due to the smaller FWHM corresponding to shorter lifetimes. Note that in the center part of the image, essentially no contrast can be observed between silver and GaAs in correspondence with a reduced contrast in the decay image (Fig. 4c). Comparison with Fig. 4a indicates a correlation of this effect with an enhanced two-photon photoemission yield. This might be the result of contamination of the GaAs interstitial part with a small silver cluster in this boundary area as result of the evaporation process. Particularly for small silver particles, effective coupling of the exciting laser light to localized plasmons can enhance photoemission yields quite significantly. These results demonstrate that the device is capable of visualizing lateral variations in the hot-electron lifetime on heterogeneous microstructured sample surfaces. We expect that implementation of an imaging energy filter will enhance the lifetime contrast significantly. The lifetime of excited electrons shows a strong dependence on excita-

tion energy, and so should the lifetime contrast. In addition to that, it has been found theoretically that the experimental autocorrelation trace can be affected by the detector energy resolution [27].

Regions of different surface composition generally feature photoemission yields that can differ substantially. This results in a very strong contrast present in the PEEM images as is, for example, evident from the images shown in Fig. 3b. Due to possible crosstalk between different areas of the detector (screen/CCD-chip), a considerable portion of the signal measured in a dark area may actually originate from bright areas. In the case of high-contrast images, our experience shows that any lifetime contrast can be blurred completely. One way to avoid this is to find a sample featuring at least approximately equivalent photoemission yields from surface areas of different chemical or structural compositions. Again, an energy filtering of the photoelectrons in the PEEM can overcome this principal limitation by selection of a suitable electron energy for imaging. This is a means to exploit the partial yield of a selected transition instead of the total yield studied in the present set-up.

#### 4 Summary

In summary we have successfully established a new experimental technique that we refer to as time-resolved two photon photoemission electron microscopy (TR-PEEM). In general, it offers a new contrast method for PEEM by the use of a femtosecond-pulsed light source. However, even more importantly, this technique is feasible to investigate the characteristics of hot-electron dynamics of surfaces at a spatial resolution of 20 nm and a time resolution of a few femtoseconds. In particular, we expect that this technique is a new probe for the physics of charge carriers in nanostructured and low-dimensional systems. Implementation of energy discrimination in terms of an imaging energy filter and/or electron-energy analyzer system is straight forward and will facilitate, in addition, time-resolved spectroscopy at high spatial resolution.

**ACKNOWLEDGEMENTS** Financial support by the DFG (grant FE 444/1 and AE 19/3-1) is gratefully acknowledged.

#### REFERENCES

- 1 R. Yen, J.M. Liu, N. Bloembergen, T.K. Yee, J.G. Fujimoto, M.M. Salour: *Appl. Phys. Lett.* **40**, 185 (1982)
- 2 R.T. Williams, R.R. Royt, J.C. Rife, J.P. Long, M.N. Kabler: *J. Vat. Sci. Technol.* **21**, 509 (1982)
- 3 W.S. Fann, R. Storz, H.W.K. Tom, J. Bokor: *Phys. Rev. B* **46**, 13 592 (1992)
- 4 C.A. Schmuttenmaer, M. Aeschlimann, H.E. Elsayed-Ali, R.J. Miller, D.A. Mantell, J. Cao, Y. Gao: *Phys. Rev. B* **50**, 8957 (1994)
- 5 R. Haight: *Surf. Sci. Rep.* **21**, 275 (1995)
- 6 R.W. Schoenlein, J.G. Fujimoto, G.L. Eesley, T.W. Capehart: *Phys. Rev. Lett.* **22**, 2596 (1988)
- 7 M. Aeschlimann, M. Bauer, S. Pawlik: *Chem. Phys.* **205**, 127 (1996)
- 8 S. Ogawa, H. Petek: *Surf. Sci.* **357–358**, 585 (1996)
- 9 T. Hertel, E. Knoesel, M. Wolf, G. Ertl: *Phys. Rev. Lett.* **76**, 535 (1996)
- 10 J. Cao, Y. Gao, H.E. Elsayed-Ali, R.J.D. Miller, D.A. Mantell: *Phys. Rev. B* **58**, 10 984 (1998)
- 11 M. Aeschlimann, C.A. Schmuttenmaer, H.E. Elsayed-Ali, R.J.D. Miller, J. Cau, Y. Gao, D.A. Mantell: *J. Chem. Phys.* **102**, 448 (1995)
- 12 J. Lehmann, M. Herschmann, W. Pfeiffer, A. Thon, S. Voll, G. Gerber: *Phys. Rev. Lett.* **85**, 2921 (2000)

- 13 J.J. Quinn, R.A. Ferrell: *Phys. Rev.* **112**, 812 (1958)
- 14 J.J. Quinn: *Phys. Rev.* **126**, 1453 (1962)
- 15 J.J. Quinn: *Appl. Phys. Lett.* **2**, 167 (1963)
- 16 P. Hawrylak, G. Eliasson, J.J. Quinn: *Phys. Rev. B* **37**, 10187 (1988)
- 17 V.A. Gasparov, R. Huguenin: *Adv. Phys.* **42**, 393 (1993)
- 18 C.A. Schmuttenmaer, C.C. Miller, J.W. Herman, J. Cao, D.A. Mantell, Y. Gao, R.J.D. Miller: *Chem. Phys.* **205**, 91 (1996)
- 19 O. Schmidt, G.H. Fecher, Y. Hwu, G. Schönhense: *Surf. Sci.* **482–485**, 687 (2001)
- 20 W. Swiech, G.H. Fecher, Ch. Ziethen, O. Schmidt, G. Schönhense, K. Grzelakowski, C.M. Schneider, R. Frömter, H.P. Oepen, J. Kirschner: *J. Elec. Spec. Rel. Phenom.* **84**, 171 (1997)
- 21 J.E. Rowe, C.V. Shank, D.A. Zwemer, C.A. Murray: *Phys. Rev. Lett.* **44**, 1770 (1980)
- 22 C.K. Chen, A.R.B. de Castro, Y.R. Shen: *Phys. Rev. Lett.* **46**, 1029 (1981)
- 23 A. Wokaun, J.G. Bergmann, J.P. Heritage, A.M. Glass, P.F. Liao, D.H. Olson: *Phys. Rev. B* **24**, 849 (1981)
- 24 J.C. Quail, H.J. Simon: *J. Opt. Soc. Am. B* **5**, 325 (1988)
- 25 Th. Bornemann, A. Otto, W. Heuer, H. Zacharias: *Surf. Sci.* **420**, 224 (1999)
- 26 K. Ertel, U. Kohl, J. Lehmann, M. Merschorf, W. Pfeiffer, A. Thon, S. Voll, G. Gerber: *Appl. Phys. B* **68**, 439 (1999)
- 27 M.J. Weida, S. Ogawa, H. Nagano, H. Petek: *J. Opt. Soc. Am. B* **17**, 1443 (2000)